УДК 539
P.A.C.S. 61.50.Ks
DOI 10.54708/26587572_2025_732299

MICROSTRUCTURE AND MICROHARDNESS OF HYDROGENATED Ti-2Fe-0.1B ALLOY A SUBJECT TO HPT IN THE SOLID SOLUTION STATE

Xujia Zhou [1a], Yuecheng Dong [2], Igor Vasilevich Alexandrov [1]

[1] Ufa University of Science and Technology, 32 Zaki Validi st., 450076 Ufa, Republic of Bashkortostan, Russia
[2] Nanjing Tech University, 30 South Puzhu Road, 211816 Nanjing, Jiangsu Province, China
[a] zhouxujia1111@163.com

ABSTRACT

This paper presents the results of a study of the microstructure and mechanical properties of a hydrogenated Ti-2Fe-0.1B alloy (in wt. %), subjected to high-pressure torsion (HPT) in a solid-solution (SS) state. The hydrogenated samples with a uniform distribution of hydrogen were obtained by holding at a temperature of 700 °C for 2 hours in a high-purity hydrogen environment and naturally cooling together with a furnace to room temperature. To form the SS state, the samples were placed in a vacuum and subjected to heat treatment. SS state with a hydrogen content of 0.3 wt.% and 0.5 wt.% was formed by holding at temperatures of 720 °C and 640 °C, respectively, for 1 hour in a vacuum followed by cooling in water. The temperature was set 10 °C above the β→α phase transformation temperature. The phase composition after SS treatment was characterized by a predominance of the β-phase and a small volume of the α-phase. The HPT was carried out at a pressure of 6 GPa at room temperature with a different number of turns. The microstructure and microhardness of the hydrogenated samples that were SS and HPT treated were investigated. The results obtained were compared with similar results obtained for samples before HPT. Microstructural analysis showed that as a result of hydrogenation and SS treatment, a β-Ti(H) phase saturated with hydrogen was formed. HPT contributed to the formation of a dispersed ω-phase and the refinement of grains in both β- and α-phases. Precipitations in the form of whiskers of the TiB phase were also observed in the microstructure. The microhardness of the alloy has increased significantly as a result of the hydrogenation, SS treatment and HPT.

KEYWORDS

Titanium alloy; hydrogenation; solid solution; HPT.

МИКРОСТРУКТУРА И МИКРОТВЕРДОСТЬ НАВОДОРОЖЕННОГО СПЛАВА Ti-2Fe-0,1B, ПОДВЕРГНУТОГО КВД В ТВЕРДОРАСТВОРНОМ СОСТОЯНИИ

Суйцзя Чжоу [1a], Юэчэн Дун [2], Игорь Васильевич Александров [1]

[1] Уфимский университет науки и технологий, Россия, Республика Башкортостан, 450076 Уфа, ул. Заки Валиди, 32
[2] Нанкинский технологический университет, Китай, 211816 г. Нанкин, ул. Южная дорога Пужу, 30
[a] zhouxujia1111@163.com

АННОТАЦИЯ

В этой статье представлены результаты исследования микроструктуры и механических свойств наводороженного сплава Ti-2Fe-0,1B (в мас.%), подвергнутого кручению под высоким давлением (КВД) в твердорастворном (ТР) состоянии. Наводороженные образцы с равномерным распределением водорода были получены путем выдержки при температуре 700 °C в течение 2 часов в среде водорода высокой чистоты и естественного охлаждения вместе с печью до комнатной температуры. Для формирования ТР состояния образцы были помещены в вакуум и подвергнуты термической обработке. При этом ТР состояния в заготовках с содержанием 0,3 масс.%H и 0,5 масс.%H были сформированы путем выдержки при температурах 720 °C и 640 °C, соответственно, в течение 1 часа в вакууме с последующим охлаждением в воде. Температура была установлена на 10 °C выше температуры фазового превращения β→α. Фазовый состав после обработки на ТР характеризовался преобладанием β-фазы и небольшим объемом α-фазы. КВД проводилось под давлением 6 ГПа при комнатной температуре с разным числом оборотов. Были исследованы микроструктура и микротвердость наводороженных образцов, прошедших обработку на ТР и КВД. Полученные результаты сравнили с аналогичными результатами, полученными для образцов до КВД. Микроструктурный анализ показал, что в результате наводороживания и обработки на ТР образовалась фаза β-Ti(H), насыщенная водородом. КВД способствовало образованию дисперсной ω-фазы и измельчению зерен как в β-, так и в α-фазах. В микроструктуре также наблюдались выделения в виде усов фазы TiB. Микротвердость сплава в результате наводороживания, обработки на ТР и КВД значительно возросла.

КЛЮЧЕВЫЕ СЛОВА

Титановый сплав; наводороживание; твердый раствор; ИПДК.

Introduction

Titanium alloys are widely used in the aerospace, marine, biomedical and another branches of industry due to their high strength-to-weight ratio and corrosion resistance. However, their applications are often limited by the lack of ductility and the challenges of microstructure refinement [1].

Fe, as a β-phase stabilizing and low-cost alloying element, has a significant regulatory effect on the microstructure and mechanical properties of Ti-2Fe-0.1B alloy [32]. The β-phase possessing the body-centered cubic crystal lattice, reduces the transition temperature from β-phase to α-phase, increases the content of high-temperature β-phase and increases the ductility. Then the hot working performance of the alloy can be improved. In addition, Fe inhibits grain growth by segregation at grain boundaries, and refines the as-cast structure by forming a Ti-Fe eutectic phase [1]. Ti-Fe phase is a CsCl-kind intermetallic compound, usually containing 20~25 wt.% Fe.

Hydrogenation causes drastic changes in the structure of Ti-2Fe-0.1B alloy. This method is known, as a temporary alloying method, has emerged as a promising approach to modify the microstructure of titanium alloys decreasing the temperature of the β→α phase transformation [2]. However, after excessive hydrogenation, the hydrogen atoms in the SS and precipitated hydrides preferentially accumulate at the grain boundaries to produce stress concentrations, accelerating the initiation and propagation of cracks. So the fracture mode of titanium alloys during tensile testing changes from ductile transgranular to brittle intergranular fracture, resulting in a sharp decrease in the ductility of hydrogenated titanium alloys at room temperature.

During the hydrogenation at high temperature the transitions $\alpha \rightarrow \alpha_H + \beta_H$, $\beta \rightarrow \beta_H$ occur. The eutectic reaction occurs during the subsequent cooling process $\beta_H \rightarrow \alpha + \delta$ and $\alpha_H \rightarrow \alpha + \delta$, martensitic α' formed with lamellar α_L. But in total after cooling the proportion of β-phase in Ti-2Fe-0.1B-0.3H alloy has been greatly increased from 4.95% to 30.1% [3].

Previous studies [7] have shown that the addition of B to Ti alloys promotes the formation of TiB whiskers, fixes grain boundaries during SS treatment, inhibits recrystallization, and enhances grain boundary strengthening. EBSD analysis confirmed that B deposition at the α/β interface improves interfacial cohesion [4].

Severe plastic deformation (SPD) methods can be used to form ultrafine-grained (UFG) states and enhance the properties of Ti alloys [5]. The average grain size decreased from 1.72 μm in the coarse grain state to 240 nm in the UFG state formed by equal channel angular pressing (ECAP) deformation of Ti-2Fe-0.1B alloy [9]. High pressure torsion (HPT) has a very strong grain refinement ability too [11]. HPT of Ti-2Fe-0.1B alloy resulted in the severe refinement of the grains from 3.5 μm in the initial state to about 20 nm after 10 turns. It was also proved that HPT can greatly increase the hardness of Ti-2Fe-0.1B alloy to the maximum 483 HV after 5 turns [1].

The optimization of the Ti-2Fe-0.1B-xH alloy could follow from the combination of strengthening due to Fe, grain refinement due to B, hydrogenation, SS and SPD.

In this paper, the synergistic effect of hydrogen content, SS treatment, and HPT on the microstructure and microhardness of Ti-2Fe-0.1B alloy was studied.

1. Materials and methods

1.1. Materials.

The low-cost titanium alloy Ti-2Fe-0.1B was made of grade 0 titanium sponge, industrial pure iron and Ti-B master alloy. The compounds were first melted twice in a vacuum arc melting furnace to obtain an ingot with a diameter of approximately 420 mm. The ingot was forged to diameter 125 mm. Surface defects and contaminated layers were removed to ensure the purity and performance consistency of subsequent processed materials. The diameter 120 mm of ingots was obtained by grinding process. The phase transition point was determined as 857±5 °C. [3] Then the diameter was decreased from 120 mm to 20 mm by continuous rolling at about 836 °C. This temperature made it easy to deform and prevented the β-phase grains from growing bigger. The chemical composition and initial grain size are shown in Table 1. The content of Fe was determined by ICP-AES (Inductively Coupled Plasma Atomic Emission Spectrometry) analyzer. The C, O, N, H elements were determined by gas analyzer. The content of B element was determined by nominal content due to high analytical difficulty and poor accuracy.

Table 1. The element composition and grain size of Ti-2Fe-0.1B alloy in the as-received state

Таблица 1. Элементный состав и размер зерна сплава Ti-2Fe-0,1B в исходном состоянии

Element / Элемент	Fe	B	C	O	N	H	Ti	Grain size, μm / Размер зерен, мкм
Wt.% / Вес.%	1.89	0.08	0.014	0.062	0.004	0.0012	Residual amount / Остаточное количество	1.72

1.2. Hydrogenation and solid solution heat treatment.

High-temperature gas-phase hydrogenation treatment was used to get the compositions of the investigated Ti-Fe-B alloy with 0.3 wt.%H and 0.5 wt.%H. Before the hydrogenation treatment, the oxide scale was removed and the surface of the billets was cleaned by ultrasonic vibration in acetone. Then the ingots were placed in the hydrogenation treatment furnace and kept at 700 °C for 2 hours in a high-purity hydrogen environment to make the hydrogen diffuse evenly. The high temperature improved the diffusion coefficient of hydrogen and accelerated the diffusion rate of hydrogen atoms from the surface to the center. The long holding time provided sufficient diffusion time for the hydrogen atoms. The hydrogen atoms have more opportunities to diffuse from the high-concentration surface area to the low-concentration internal area until the concentration gradient disappeared and the homogenization was achieved. Then furnace was cooled to room temperature. The hydrogen content was determined by weighing the ingots before and after the hydrogenation treatment. The analytical balance with an accuracy of 0.00001 g was used.

The ingots were put in vacuum with the pressure under 5.0×10^{-3} Pa and heat-treated for 1 hour. The temperature was set 10 °C above the hydrogen-containing $\beta \rightarrow \alpha$-phase transformation point. It was put as 720 °C for 0.3%H and 640 °C for 0.5%H [3]. Then the ingots were water-cooled.

1.3. High-pressure torsion.

Before HPT, the as-received and hydrogenated ingots were cut into the disks with a diameter of 20 mm and a thickness of 1.5 mm. Then the disks were polished to about 1 mm using sandpaper of 80#, 240#, 400#, 600#, 800#, 1200# and 1500# in turn, so that the size of the specimen meets the dimensional requirements for HPT.

The samples were a subject to HPT. The pressure of 6 GPa was applied at room temperature. The numbers of turns were selected as 1/2, 1, 5, and 10.

Fig. 1. Hydrogen treatment furnace

Рис. 1. Печь для наводороживания

Fig. 2. High pressure torsion equipment diagram

Рис. 2. Схема оборудования для кручения под высоким давлением

1.4. Characterization methods.

1.4.1. SEM observation.

1 mm thick discs with ⌀ 20 mm were polished with sandpaper to remove the surface oxide layer, grounded until the surface became smooth, then mechanically polished to make the surface of the sample mirror-like, cleaned, and dried for the observation by backscatter analysis/ The scanning electron microscope JEOL JSM-6510 was used.

1.4.2. XRD analysis.

1 mm thick discs with ⌀ 20 mm were polished with sandpaper to remove the surface oxide layer, grounded until the surface became smooth, mechanically polished, cleaned, and dried before XRD testing. The investigations were conducted on the diffractometer Rigaku RINT 4200. The X-ray diffraction analysis of the samples was carried out by Cu-Kα radiation at room temperature. The 2θ range from 20 to 80° was selected. The scanning speed was 5°/min. At the end of the experiment, the data were exported and analyzed by EVA and Jade software to confirm the possible phases and corresponding crystal structures. The analysis data were re-plotted by Origin software. The identified phases were labeled in the Origin diagram.

1.4.3. Vickers hardness test.

1 mm thick discs with ⌀ 20 mm were polished with sandpaper to remove the surface oxide layer, grounded until the surface became smooth, and machine polished to make the surface of the sample mirror-like, cleaned and dried for microhardness testing. The model of the equipment used for the microhardness test was Emco-Test Durascan 50. The load was HV0.2 (i.e. 0.2 kgf), and the holding time was 10 s. At the end of the experiment, the data were exported, and then re-plotted using Origin software. The identified phases were labeled in the Origin diagram.

2. Results and discussion

2.1. Microstructural evolution.

According to the SEM analysis, after hydrogenation and SS treatment blocks of β-phase grains, needle-like α-phase grains, and black α'-phase grains appear in the image (Fig. 3). The original β-phase area enlarged because the hydrogenation reduced the phase transition temperature β → α of the alloy. Martensite α'-phase (lath-like structure) appeared due to cooling in water after SS treatment. The β → α' martensitic phase transformation refined the microstructure. After HPT, a large number of dislocations appear in

the alloy structure which increases with the number of HPT turns [5].

During HPT, the transition from the α-phase to the ω-phase occurs [27]. The ω-phase grains are extremely small in size (2–10 nm) [6]. They are usually evenly distributed in the matrix. A large number of the ω-phase appears in the hydrogenated SS ingots. When the number of HPT turns is 1/2 turn, ω-phase appeared in the alloy. The volume fraction of it is about 38%. With the increase of the number of HPT turns, the volume fraction of the ω-phase continues to increase. After 5 turns, the volume fraction reached the maximum about 80%. When the number of HPT turns continues to increase the volume fraction of ω-phase begins to decrease.

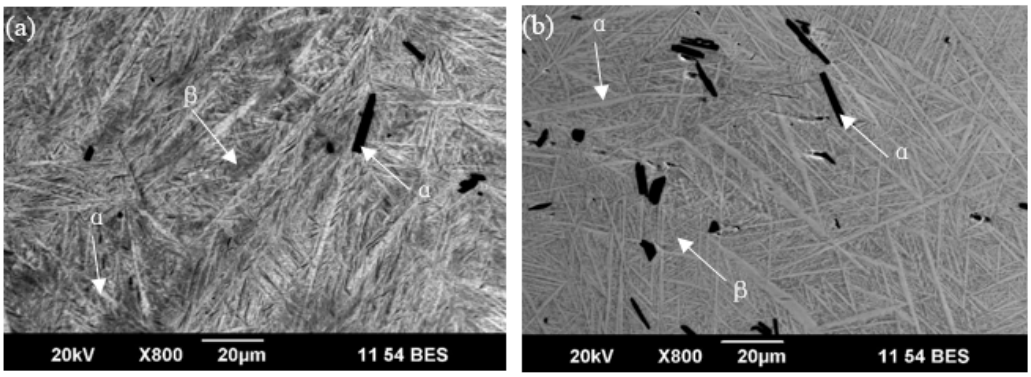

Fig. 3. SEM of Ti-2Fe-0.1B-xH alloy after SS treatment: *a – Ti-2Fe-0.1B-0.3H; b – Ti-2Fe-0.1B-0.5H*

Рис. 3. РЭМ сплава Ti-2Fe-0,1B-xH после обработки на твердый раствор: *a – Ti-2Fe-0,1B-0,3H; b – Ti-2Fe-0,1B-0,5H*

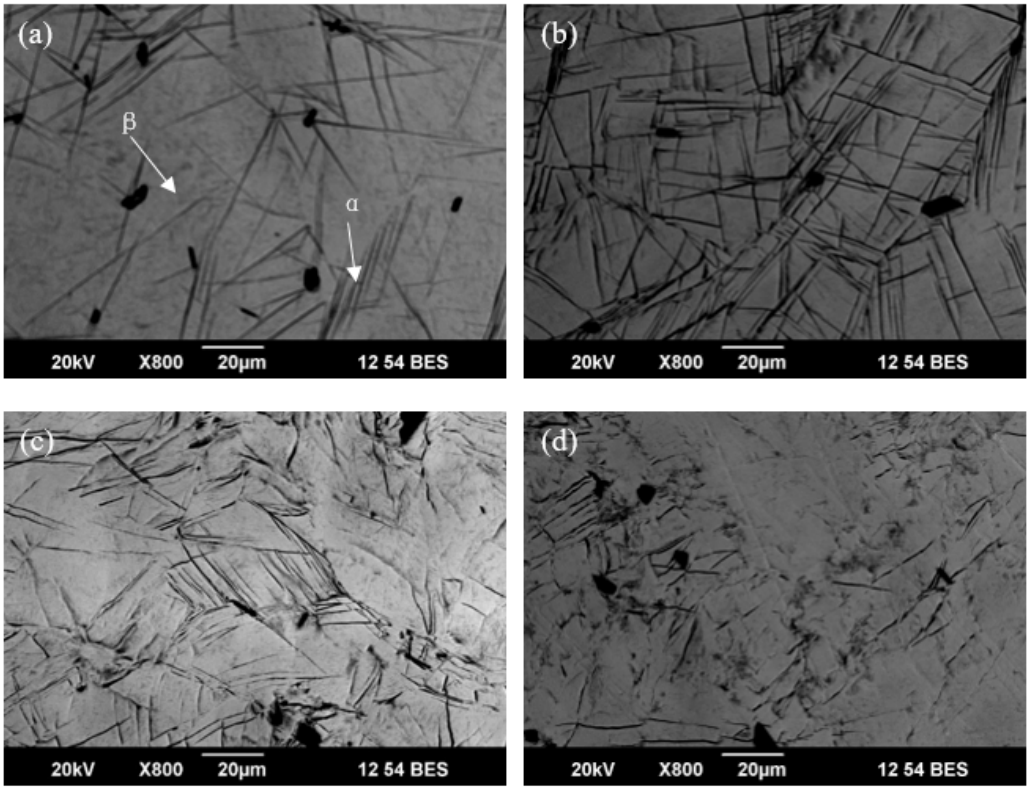

Fig. 4. SEM of Ti-2Fe-0.1B-0.3H alloy after HPT: *a – 1/2 turns; b – 1 turn; c – 5 turns; d – 10 turns*

Рис. 4. СЭМ сплава Ti-2Fe-0,1B-0,3H после КВД: *a – 1/2 оборот; b – 1 оборот; c – 5 оборотов; d – 10 оборотов*

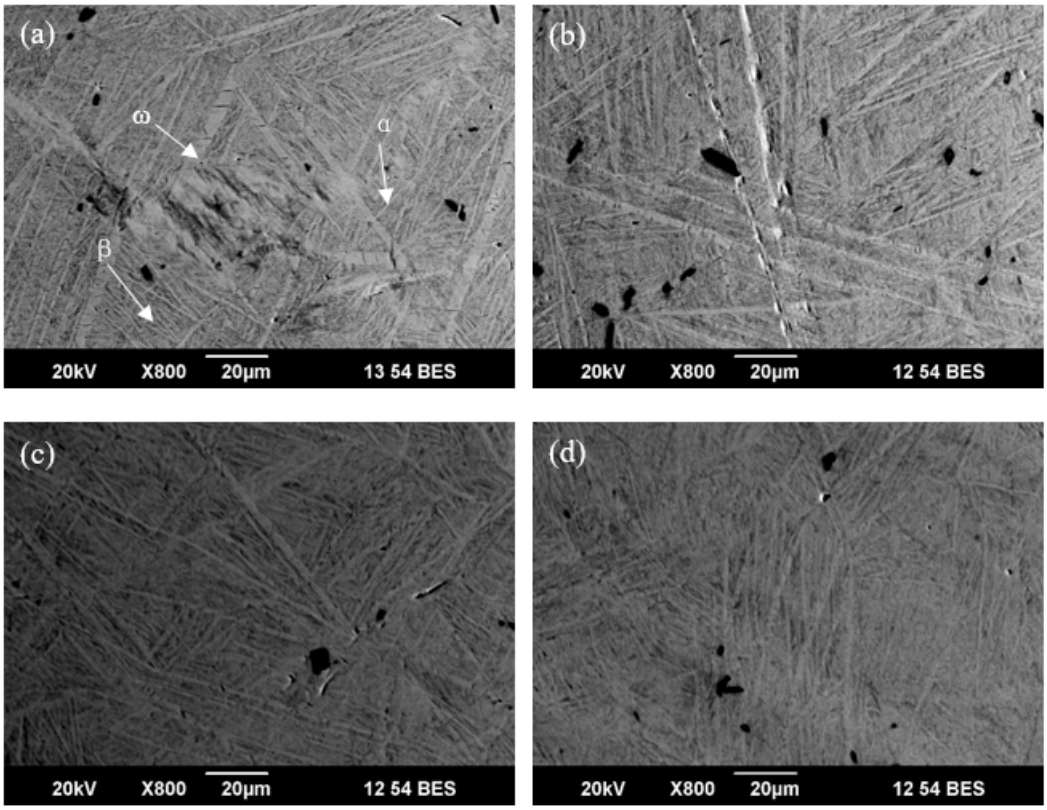

Fig. 5. SEM of Ti-2Fe-0.1B-0.5H alloy after HPT: *a – 1/2 turns; b – 1 turn; c – 5 turns; d – 10 turns*

Рис. 5. СЭМ сплава Ti-2Fe-0,1B-0,3H после НРТ: *a – 1/2 оборота; b – 1 оборот; c – 5 оборотов; d – 10 оборотов*

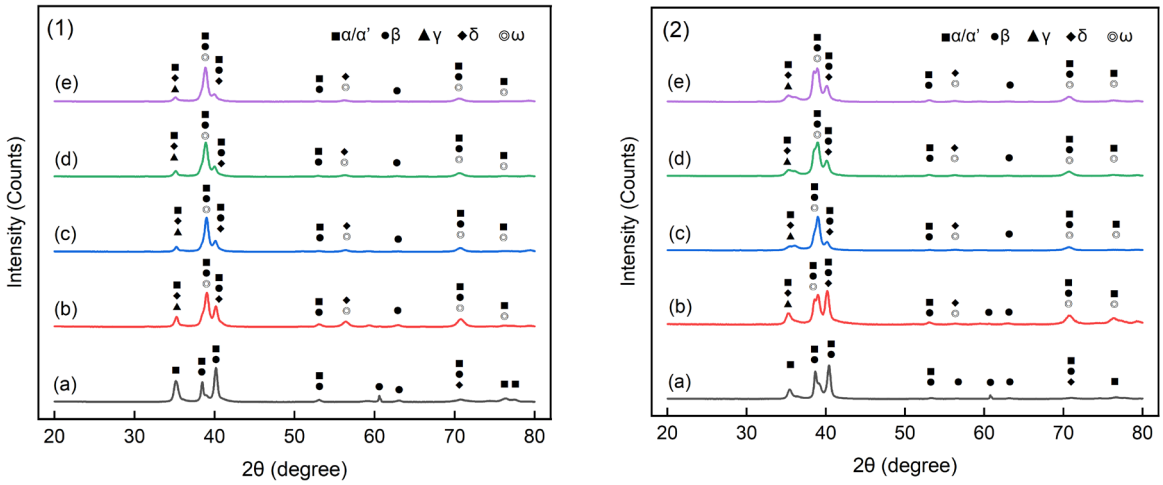

Fig. 6. XRD patterns of Ti-2Fe-0.1B-xH alloy after SS treatment:
(1) Ti-2Fe-0.1B-0.3H; (2) Ti-2Fe-0.1B-0.5H (a–e). The numbers of HPT turns are 0, 0.5, 1, 5, 10

Рис. 6. Рентгенограммы сплава Ti-2Fe-0,1B-xH после обработки на ТР:
(1) Ti-2Fe-0,1B-0,3H; (2) Ti-2Fe-0,1B-0,5H (a–e). Число оборотов при КВД составляет 0, 0,5, 1, 5, 10

The XRD patterns of Ti-2Fe-0.1B-xH alloy are shown in Fig. 6. The relative intensity of the β-Ti peaks increases with the increase of hydrogen content, indicating that the addition of hydrogen improves the stability of the β-phase. Then more β-phase is retained when the ingot is cooled to room temperature. A hydride diffraction peak with a face-centered cubic structure is found near 70°. It corresponds to the hydrides with the chemical composition $TiH_{1.5}$-$TiH_{1.97}$. The addition of hydrogen leads to the increase of hydrogen concentration in the lattice structure, and the reaction with titanium atoms at high hydrogen concentration forms a large number of hydrides.

A large volume of the ω-phase appears in the alloy with the increase in the number of HPT turns. The volume fraction of the ω-phase continues to increase, reaching the maximum after 5 turns. In case of further increase of the number of HPT turns up to 10 turns, it is found that the volume fraction of the ω-phase decreases. With the increase of the strain, the dislocation density becomes extremely high, and the transition of the ω-phase is mechanically inhibited by the stress field formed by the dislocations. According to the increase of the full width at half-maximum (FWHM), grain size decreases with the number of HPT turns.

2.2. Microhardness.

It is evident from Fig. 7 that the microhardness distribution along the diameter of the disks for the alloy with the different concentration of H (Ti-2Fe-0.1B-0.3H and Ti-2Fe-0.1B-0.5H) in the hydrogenated SS state before HPT is relatively uniform, ranging from 360 to 380 HV. The average values are 368 HV and 367 HV, respectively. However, the microhardness of the sample after HPT treatment is very uneven in the radial direction, and the curve is roughly V-shaped. The microhardness value increases with the increase of the distance from the center of the disk. After the HPT treatment, the microhardness increased with the increase of the number of turns. After 10 turns the microhardness of the alloy with the different content of H (Ti-2Fe-0.1B-0.3H and Ti-2Fe-0.1B-0.5H) reached 499 HV and 498 HV, respectively. It is 73.75% and 73.69% higher than that of the hydrogenated SS samples without HPT processing. However, the saturated microhardness of Ti-6Al-4V and pure titanium after HPT is only 435 HV and 350 HV [1].

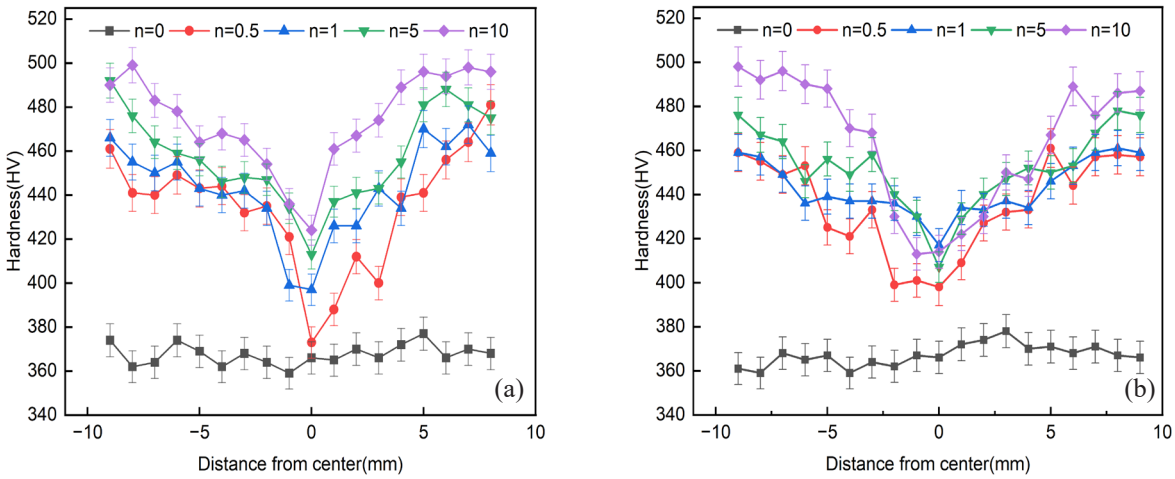

Fig. 7. The microhardness distribution along the diameter of the disks of the alloy with the different content of H: *a – Ti-2Fe-0.1B-0.3H; b – Ti-2Fe-0.1B-0.5H*

Рис. 7. Распределение микротвердости вдоль диаметра дисков сплава с различным содержанием водорода: *a – Ti-2Fe-0,1B-0,3H; b – Ti-2Fe-0,1B-0,5H*

It can be seen that the hardness increases as the strain applied to the sample increases. It is mainly caused by the grain refinement by HPT and the dislocation density increase [5]. Even after 1/2 turn of HPT processing, the microhardness of the sample increased significantly compared to the hydrogenated SS sample before HPT. The hardness of the center of the disc was significantly lower than that of the edges, but still higher than that before HPT. In general, the hardness changes tend to increase from the center along the radial direction to the edge. This is due to the fact that the strain of the disc sample increases from the central region along the edge after high-pressure torsion.

Conclusion

1. The β-phase of SS-treated alloy has a higher volume fraction. Hydrogen reduces the phase transition point temperature of titanium alloys α/β. As a result, SS treatment can be carried out at lower phase transition point temperatures. The excessive growth of β grains was inhibited.

2. In the process of HPT, the transition from the α-phase to the ω-phase occurs. About 80% of the ω-phase appears in the SS ingots. With the increase in the number of HPT turns the volume fraction of the ω-phase continues to increase, and reaches the maximum after 5 turns. Then the volume fraction of the ω-phase begins to decrease as the number of HPT turns continues to increase up to 10.

3. The saturated microhardness (499 HV, 498 HV) of the alloy hydrogenated alloy (Ti-2Fe-0.1B-0.3H and Ti-2Fe-0.1B-0.5H) after SS treatment and HPT is 3% higher than that of Ti-2Fe-0.1B alloys (483 HV) after high-pressure torsion.

Acknowledgments / Благодарности

This research was funded by the Russian Science Foundation, grant No. 23-43-00041 (https://rscf.ru/project/23-43-00041/ accessed on 21 August 2024), and the National Natural Science Foundation of China, grant No. 52261135539.

Данные научные исследования были поддержаны Российским научным фондом в рамках гранта № 23-43-00041 (https://rscf.ru/project/23-43-00041/, дата обращения: 21 августа 2024 г.) и Государственным фондом естественных наук Китая в рамках гранта № 52261135539.

REFERENCES

1. Wang Y., Jin Y., Chen K., Liang Z., Sitdikov V.D., Dong Y., Chang H, Alexandrov I.V. Phase transformation and mechanical properties of nanocrystalline Ti–2Fe-0.1B alloy processed by high pressure torsion // Journal of Materials Research and Technology. 2024. Vol. 31.P. 1853–1863. DOI: 10.1016/j.jmrt.2024.06.164.

2. O.N. Senkov, F.H. Froes, Thermohydrogen processing of titanium alloys // International Journal of Hydrogen Energy. Volume 24. Issue 6. 1999. Pages 565-576. ISSN 0360-3199.DOI: 10.1016/S0360-3199(98)00112-8.

3. Zhang B., Wang Y., Alexandrov I.V., Sun Z., Dong Y., Valiev R.Z., Wang Y., Zhou L. Effect of hydrogen on microstructure evolution and deformation behaviors of Ti-2Fe-0.1B alloy // Journal of Alloys and Compounds. 2022. Vol. 900. Art. 163473. DOI: 10.1016/j.jallcom.2021.163473.

4. Li C., Zhang X., Li Z., Zhou K. Effect of heat treatment on microstructure and mechanical properties of ultra-fine grained Ti-55511 near β titanium alloy // Rare Metal Materials and Engineering. 2015. Vol. 44. Iss. 2. P. 327–332. DOI: 10.1016/S1875-5372(15)30029-1.

5. Zhengjie, L., et al. The ultrafine-grained titanium and biomedical titanium alloys processed by severe plastic deformation (SPD) // SOJ Materials Science & Engineering: 2013. Vol. 1.1. P. 1-5.

6. Lin C., Yu J., Yin G., Zhang A., Zhao Z., Huang S., Zhao Y., Guo L. Research progress of ω phase transition in titanium alloy // Material Review. 2017. Vol. 31. Iss. 5. P. 72-76

7. Niu J., Dai G., Dan Z., Dong Y., Chang H., Alexandrov I. V., Zhou L. Microstructure and mechanical properties of B modified Ti–Fe alloy manufactured by casting, forging and laser melting deposition // Composites Part B: Engineering. 2021. Vol. 216. Art. 108854. DOI: 10.1016/j.compositesb.2021.108854.

8. Guo C., Guo Y., Dan Z., Chang H.. Electrochemical and passive behaviors of Ti-Fe-B alloy manufactured via casting, forging and additive manufacturing // Materials Characterization. 2023. Vol. 196. Art. 112530. DOI: 10.1016/j.matchar.2022.112530.

9. Wang C., Sun Y., Mi Y. Dong Y. Chang H. 1 andI. V. Alexandrov Low-cycle fatigue behavior and

fracture characteristics of low-cost Ti-2Fe-0.1B alloy // Metals. 2023. Vol. 13. No. 7. Art. 1208. DOI: 10.3390/met13071208.

10. Huang S., Jin Y., Wang Y., Dong Y., Chang H., Alexandrov I.V. Stress corrosion cracking of ultrafine-grained Ti-2Fe-0.1B alloying after equal channel angular pressing // Metals. 2023. Vol. 13. No. 7. Art. 1316. DOI: 10.3390/met13071316.

11. Jorge A.M., Roche V.Jr., Pérez D.A.G., Valiev R. Z. Nanostructuring Ti-alloys by HPT: Phase transformation, mechanical and corrosion properties, and bioactivation // Materials Transactions. 2023. Vol. 64, Iss. 7. P. 1306–1316. DOI: 10.2320/matertrans.MTMF2022014.

12. Wang Y., Li X., Alexandrov I.V., Ma L., Dong Y., Valiev R.Z., Chang H., Zhang B., Wang Y., Zhou L., Hu Zh. Impact of equal channel angular pressing on mechanical behavior and corrosion resistance of hot-rolled Ti-2Fe-0.1B alloy // Materials. 2020. Vol. 13(22). No. 5117. DOI: 10.3390/ma13225117.

13. Guo C., Niu J., Dai G., Guo Y., Dan Z., Chang H. Electrochemical and passive behaviors of Ti-Fe-B alloy manufactured via casting, forging and additive manufacturing // Materials Characterization. 2023. Vol. 196. Art. 112530. DOI: 10.1016/j.matchar.2022.112530.

14. Gaurav S., Upadrasta R. Boron modified titanium alloys // Progress in Materials Science. 2020. Vol. 111. Art. 100653. DOI: 10.1016/j.pmatsci.2020.100653.

15. Aparicio-Fernández R., Szczepaniak A., Springer H., Raabe D. Crystallisation of amorphous Fe-Ti-B alloys as a design pathway for nano-structured high modulus steels // Journal of Alloys and Compounds. 2017. Vol. 704. P. 565–573. https://doi.org/10.1016/j.jallcom.2017.02.077.

16. Ratochka I.V., Naydenkin E.V., Mishin I.P., Lykova O.N., Zabudchenko O.V. Low-temperature superplasticity of ultrafine-grained near β titanium alloy // Journal of Alloys and Compounds. 2022. Vol. 891. Art. 161981. DOI: 10.1016/j.jallcom.2021.161981.

17. Du Z., Liu J., Li G., Lv K., Liu G., Yan L., Chen Y. Low-temperature superplastic behavior of beta titanium alloy // Materials Science and Engineering: A. 2016. Vol. 650. P. 414–421. DOI: 10.1016/j.msea.2015.10.065.

18. Estrin Y., Vinogradov A. Extreme grain refinement by severe plastic deformation: A wealth of challenging science // Acta Materialia. 2013. Vol. 61. Iss. 3. P. 782–817. DOI: 10.1016/j.actamat.2012.10.038.

19. Dai G., Cui Y., Zhou D., Guo Y., Chang H., Zhou L. Hot deformation behavior and mechanistic understanding of new TF400 titanium alloy // Metals. 2019. Vol. 9(12). Art. 1277. DOI: 10.3390/met9121277.

20. Guo C., Dai G., Niu J., Guo Y., Sun Z., Chang H., Zhang Q. Fe nanoparticles modified pure Ti alloy on microstructure evolution and fine crystallization mechanism fabricated by additive manufacturing // Journal of Materials Research and Technology. 2023. Vol. 26. P. 5860–5872. DOI: 10.1016/j.jmrt.2023.08.221.

21. Valiev R.Z., Estrin Y., Horita Z. Langdon T.G., Zehetbauer M., Zhu Y.T. Correction to: Producing bulk ultrafine-grained materials by severe plastic deformation // JOM. 2020. Vol. 72(9). P. 3304. DOI: 10.1007/s11837-020-04194-5.

22. Wilches Pena L.V., Wang L., Mellor B.G., Schwedt A., Mayer J., Holweger W. Characterisation of white etching structures formed in annealed AISI 52100 through high pressure torsion (HPT) // Tribology International. 2023. Vol. 184. Art. 108432. DOI: 10.1016/j.triboint.2023.108432.

23. Kilmametov A., Ivanisenko Y., Straumal B., Mazilkin A.A., Gornakova A.S., Kriegel M.J., Fabrichnaya O.B., Rafaja D., Hahn H. Transformations of α' martensite in Ti–Fe alloys under high pressure torsion // Scripta Materialia. 2017. Vol. 136. P. 46–49. DOI: 10.1016/j.scriptamat.2017.04.010.

24. Esteban P.G., Ruiz-Navas E.M., Gordo E. Influence of Fe content and particle size the on the processing and mechanical properties of low-cost Ti–xFe alloys // Materials Science and Engineering: A. 2010. Vol. 527(21–22). P. 5664–5669. 10.1016/j.msea.2010.05.026.

25. Chen N., Hu S., Setyawan W., Gwalani B., Sushko P.V., Mathaudhu S.N. Formation and dissociation of shear-induced high-energy dislocations: insight from molecular dynamics simulations // Model. Simul. Mat. Sci. Eng. 2022. Vol. 30. Art. 25012. DOI: 10.1088/1361-651X/ac44a5.

26. Alleman C., Medlin D., Sills R. Energy and stochasticity: the yin and yang of dislocation patterning // Mater. Res. Lett. 2023. Vol. 4. P. 289–295. DOI: 10.1080/21663831.2022.2149283.

27. Tong L., Kent D., Gang S., Hongwei L., Fries SG., Ceguerra A.V., Dargusch M.S., Cairney J.M. Nucleation driving force for ω-assisted formation of α and associated ω morphology in β-Ti alloys // Scripta Materialia. 2018. Vol. 155. P. 149–154. DOI: 10.1016/j.scriptamat.2018.06.039.

28. Mirmahdi S.H., Javanbakht M., Barchiesi E. Surface layer effect on high pressure phase growth in a bicrystal: phase field model and simulations // Continuum Mech. Thermodyn. 2024. Vol. 36. P. 1565–1577. DOI: 10.1007/s00161-024-01316-1.

29. Dai G., Cui Y., Zhou D., Guo Y., Chang H., Zhou L. hot deformation behavior and mechanistic understanding of new TF400 titanium alloy //Metals. 2019. Vol. 9(12). Art. 1277. DOI: 10.3390/met9121277.

30. Wu L., Jia C., Han S., Li N., Ni D., Xiao B., Ma Z., Fu M., Wang Y., Zeng Y. Superplastic deformation behavior of lamellar microstructure in a hydrogenated friction stir welded Ti-6Al-4V joint // Journal of Alloys

and Compounds. 2019. Vol. 787. P. 1320–1326. DOI: 10.1016/j.jallcom.2019.02.182.

31. Sun Z., Qi F., Guo Y., Wang Y., Chang H., Wu F., Chen W., Ji X. The effect of hydrogen on the grain refinement and mechanisms for Ti6Al4V alloys during laser melting deposition // Journal of Alloys and Compounds. 2021. Vol. 877. Art. 160122. DOI: 10.1016/j.jallcom.2021.160122.

32. Niu J., Guo Y., Li k., Liu W., Dan Z., Sun Z., Chang H., Zhou L. Improved mechanical, bio-corrosion properties and in vitro cell responses of Ti-Fe alloys as candidate dental implants // Materials Science and Engineering: C. 2021. Vol. 122. Art. 111917. DOI: 10.1016/j.msec.2021.111917.

33. Sandlöbes S., Korte-Kerzel S., Raabe D. On the influence of the heat treatment on microstructure formation and mechanical properties of near-α Ti-Fe alloys // Materials Science and Engineering: A. 2019. Vol. 748. P. 301–312. DOI: 10.1016/j.msea.2018.12.071.